ADVANCED FUNCTIONAL MATERIALS
www.afm-journal.de

Exciton and Polaron Quenching in Doping-Free Phosphorescent Organic Light-Emitting Diodes from a Pt(II)-Based Fast Phosphor

Qi Wang, Iain W. H. Oswald, Michael R. Perez, Huiping Jia, Bruce E. Gnade, and Mohammad A. Omary**

By introducing a neat Pt(II)-based phosphor with a remarkably short decay lifetime, a simplified doping-free phosphorescent organic light-emitting diode (OLED) with a forward viewing external quantum efficiency (EQE) and power efficiency of 20.3 ± 0.5% and 63.0 ± 0.4 lm W^{-1}, respectively, is demonstrated. A quantitative analysis of how triplet-triplet annihilation (TTA) and triplet-polaron annihilation (TPA) affect the device EQE roll-off at high current densities is performed. The contributions from loss of charge balance associated with charge leakage and field-induced exciton dissociation are found negligible. The rate constants k_{TTA} and k_{TPA} are determined by time-resolved photoluminescence experiments of a thin film and an electrically-driven unipolar device, respectively. Using the parameters extracted experimentally, the EQE is modeled versus electric current characteristics of the OLEDs by taking both TTA and TPA into account. Based on this model, the impacts of the emitter lifetime, quenching rate constants, and exciton formation zone upon device efficiency are analyzed. It is found that the short lifetime of the neat emitter is key for the reduction of triplet quenching.

1. Introduction

Phosphorescent organic light-emitting diodes (PhOLEDs) represent a promising technology for both solid-state lighting and display applications because of their ability to convert 100% of the injected electrons into photons by harvesting the energy of both singlet and triplet excitons.[1–3] Although various methods have been proposed to improve the performance for PhOLEDs,[4–6] host-guest doping is required for all of today's state-of-the-art PhOLEDs.[1–6] This is because the long lived triplets in common phosphorescent dyes tend to aggregate and induce strong self-quenching in the neat form.[7] Doped PhOLEDs with very high external quantum efficiency (EQE) for blue,[8] green,[9] orange,[5d] and white emission,[10] have been reported in recent years; however, problems remain for the doping technique. First, precise control of doping is a very complicated and time-consuming process. Additionally, doping system could cause parasitic exchange energy losses in power efficiency (PE), resulting from the host-to-guest energy transfer.[11] Although doping-free PhOLEDs (DF-PhOLEDs) provide a promising alternative to overcome both problems,[12–14] the highest PE of DF-PhOLEDs reported to date is 45 lm W^{-1},[14a] which still cannot compete with that achieved in doped PhOLEDs (61.7 lm W^{-1}) with similar spectrum (orange/red emission).[5d]

Furthermore, in typical PhOLEDs the device EQE decreases rapidly from its peak value with increasing current because of the long triplet lifetime (1–10 μs) of common phosphorescent dyes.[3] This efficiency roll-off in PhOLEDs can be attributed to the following factors: triplet-triplet annihilation (TTA), triplet-polaron annihilation (TPA), loss of charge balance, and field-induced exciton dissociation.[15] Studies on the four processes in doped PhOLEDs have been extensively reported. Baldo and co-workers reported that TTA is the dominant factor for the EQE roll-off in a Pt-based PhOLED because the emitter possesses a rather long photoluminescence (PL) lifetime (>80 μs).[16] Reineke et al. found that TTA and TPA coexist in their Ir(III)-based device with a short PL lifetime of ≈1 μs.[17] The influence of reduced charge balance on device efficiency was reported by Giebink et al.[18] Recently, Aziz and co-workers proposed that TPA could be the only source for efficiency roll-off in some devices.[19] Besides, field-induced quenching has also been observed by Kalinowski et al. and other groups.[20] As can be seen, studies on triplet quenching processes have been mainly involved in doped devices. Corresponding research in DF-PhOLEDs is rare,[15e] though this is needed and urgent information for the further development of non-doped PhOLEDs.

In this study, simple bilayer DF-PhOLEDs with the highest efficiencies yet reported for such device types (20.3 ± 0.5% for

Dr. Q. Wang, I. W. H. Oswald, Prof. M. A. Omary
Departments of Chemistry and Physics
and Center for Advanced Research
and Technology (CART)
University of North Texas
Denton, TX 76203, USA
E-mail: Omary@unt.edu
M. R. Perez, Dr. H. Jia, Prof. B. E. Gnade
Department of Materials Science and Engineering
and Erik Jonsson School of Engineering and Computer Science
University of Texas at Dallas
Richardson, TX 75083, USA
E-mail: Gnade@utdallas.edu

DOI: 10.1002/adfm.201300699

EQE and 63.0 ± 0.4 lm W^{-1} for PE) are demonstrated by using a Pt(II)-based emitter with fast decay. We then focus on the triplet quenching processes in this device to determine the origin of the efficiency roll-off at high current densities. The contributions from field-induced exciton dissociation and loss of charge balance associated with charge leakage are found negligible. A mathematical description of the EQE roll-off, combining both TTA and TPA, is proposed to model the experimental data. Using this model, the influence of several parameters like quenching rate constants, lifetime and length of exciton recombination zone on the device efficiency is also discussed.

2. Results

2.1. Doping-Free PhOLEDs

Here, neat bis[3,5-bis(2-pyridyl)-1,2,4-triazolato]platinum(II), [$Pt(ptp)_2$], is selected as the emitting layer (EML) because the neat $Pt(ptp)_2$ film exhibits a quantum yield of nearly 100%.[2,21,22] The device structure employed is ITO/1,1-bis[(di-4-tolylamino)phenyl]cyclohexane (TAPC) (X nm)/$Pt(ptp)_2$ (100 nm)/LiF/Al (see device energy-levels in Supporting Information Figure S1),[24–26] with the TAPC thickness changing from 0 to 100 nm.[23] For this type of device, the TAPC layer plays an important role in achieving high efficiency because: 1) it can serve as an efficient hole-transporting and electron/exciton-blocking layer (Supporting Information Figure S1); 2) the charge balance of the device can be tuned by changing the thickness of this layer.[24] **Figure 1** and **Table 1** summarize the performance characteristics of this family of devices. Electroluminescence (EL) peaks of the resulting devices are around 580 nm. At a TAPC thickness of 50 nm, the device performance reaches the optimum with a forward viewing PE of 63.0 ± 0.4 lm W^{-1} and EQE of 20.3 ± 0.5%. Remarkably, this is even superior to that achieved in today's state-of-the-art PhOLEDs (with similar EL spectrum) which include much more sophisticated device structures.[5d] Table 1 also shows that our devices exhibit a rather low turn-on voltage of 2.2 V (at 1 cd m^{-2}) in a wide range of TAPC thicknesses. This is a prerequisite to achieving such high PEs in these devices.[2,22] Furthermore, compared to most doped PhOLEDs the efficiency roll-off in our devices is low, e.g., the EQEs decrease by less than 5% at a high brightness of 1000 cd m^{-2}. In the following sections the triplet quenching mechanisms that can lead to efficiency roll-off in these DF-PhOLEDs will be discussed, including TTA, TPA, field-induced quenching and loss of charge balance.[16–20]

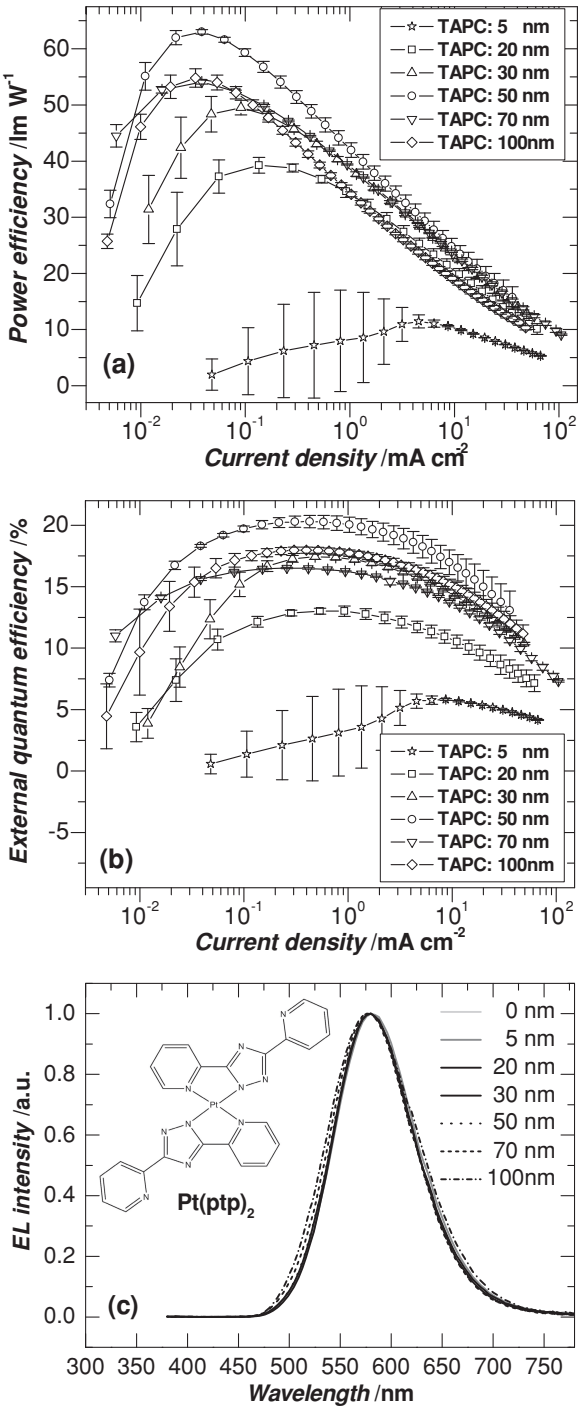

Figure 1. Forward viewing power efficiency, a) and external quantum efficiency, b) of devices with the structure of ITO/TAPC (5, 20, 30, 50, 70, 100 nm)/$Pt(ptp)_2$ (100 nm)/LiF/Al. c) Electroluminescence spectra of the above devices (including the device with TAPC thickness = 0 nm) at a voltage of 6 V. Inset: the molecular structure of $Pt(ptp)_2$.

2.2. Triplet-Triplet Annihilation

In a triplet-triplet quenching process one participant loses energy and goes back to the ground state whereas the second participant is promoted to a higher state that ultimately relaxes to the emitting triplet ($^3M^* + {}^3M^* \xrightarrow{k_{TTA}} {}^3M^* + M$).[27] Here, M represents the ground state of the molecule and k_{TTA} is the rate constant for the TTA process. The PL transient method provides a means to quantify the quenching rate in TTA.[16,17] Under a short-pulse optical excitation, the time development of the triplet exciton population can be expressed as[16]

$$\frac{d\left[{}^3M^*\right]}{dt} = -\frac{\left[{}^3M^*\right]}{\tau} - \frac{1}{2}k_{TTA}\left[{}^3M^*\right]^2 \quad (1)$$

Table 1. Performance characteristics of PhOLEDs based on neat $Pt(ptp)_2$. Each device is constructed with ITO anode and LiF/Al cathode (ITO/organic layer(s)/LiF/Al), with the combination of the rest organic layer(s) shown in column 1. Parameters listed are turn-on voltage (V_t, defined as the drive voltage at 1 cd m^{-2}), power efficiency (PE), and external quantum efficiency (EQE). Device efficiencies are listed at peak performance and at brightness of 500, 1000 cd/m^2.

Device	V_t [V]	PE [lm/W] (at peak, 500 cd m^{-2}, 1000 cd m^{-2})	EQE [%] (at peak, 500 cd m^{-2}, 1000 cd m^{-2})
TAPC(0 nm)/$Pt(ptp)_2$ (100 nm)	3.4	0.08 ± 0.01, -, -[a)]	0.07 ± 0.01, -, -
TAPC(5 nm)/$Pt(ptp)_2$(100 nm)	2.2	11.5 ± 1.2, 11.0 ± 3.0, 10.9 ± 0.6	5.8 ± 0.1, 5.2 ± 0.6, 5.8 ± 0.1
TAPC(20 nm)/$Pt(ptp)_2$(100 nm)	2.2	39.3 ± 1.4, 32.6 ± 1.1, 28.3 ± 1.1	13.0 ± 0.2, 12.8 ± 0.2, 12.2 ± 0.5
TAPC(30 nm)/$Pt(ptp)_2$(100 nm)	2.2	49.5 ± 1.3, 38.4 ± 0.4, 33.5 ± 0.2	17.4 ± 0.2, 17.3 ± 0.2, 16.7 ± 0.1
TAPC(50 nm)/$Pt(ptp)_2$(100 nm)	2.2	63.0 ± 0.4, 45.0 ± 1.2, 39.4 ± 1.3	20.3 ± 0.5, 20.2 ± 0.6, 19.8 ± 0.6
TAPC(70 nm)/$Pt(ptp)_2$(100 nm)	2.2	54.0 ± 0.4, 39.1 ± 0.1, 34.3 ± 0.1	16.5 ± 0.1, 16.2 ± 0.1, 15.7 ± 0.1
TAPC(100 nm)/$Pt(ptp)_2$(100 nm)	2.4	54.8 ± 1.6, 35.2 ± 0.5, 29.5 ± 0.4	18.0 ± 0.2, 17.7 ± 0.2, 17.3 ± 0.3

[a)]The maximum brightness of the device based on pure $Pt(ptp)_2$ is only 204.6 cd m^{-2}. This device suffers from strong exciton quenching by the ITO anode because neat $Pt(ptp)_2$ is an electron-transporting material, making the main recombination zone shift to the interface between $Pt(ptp)_2$ and ITO.

which can be solved to attain:

$$L_{TTA}(t) = \frac{L(0)}{\left(1 + [^3M^*(0)]\frac{k_{TTA}\tau}{2}\right)e^{t/\tau} - [^3M^*(0)]\frac{k_{TTA}\tau}{2}} \quad (2)$$

Here, τ is the phosphorescence lifetime of the emitter and L is the luminescence intensity. Equation (2) is based on one assumption that L is linearly proportional to the concentration of excited states (i.e., $L(t) \propto [^3M^*(t)]/\tau$).[16] For this measurement, a 100 nm neat film of $Pt(ptp)_2$ is excited by the pulsed N_2 laser. **Figure 2** shows the PL time decay of the thin film under different excitation intensities. The TTA rate constant k_{TTA} and lifetime τ can be derived by fitting the decay curves (solid lines in Figure 2) using Equation (2). **Figure 3** shows the calculated k_{TTA} and τ as a function of the initial exciton density, $[^3M^*(0)]$. The mean values of k_{TTA} and τ are calculated to be (6.5 ± 3.2) ×10^{-12} cm^3 s^{-1} and 469 ± 13 ns, respectively.

The magnitude of k_{TTA} in neat $Pt(ptp)_2$ herein is comparable to that in many doped phosphorescent systems reported previously,[15a,16,17,28] falling in the same ≈10^{-12} cm^3 s^{-1} order of magnitude and corresponding to equal initial exciton densities (≈10^{16}–10^{17} cm^{-3}). This occurs despite the shorter distance between molecules in neat $Pt(ptp)_2$ (<1 nm vs 2.2 nm in a 10% doping system).[29] The shorter lifetime of neat $Pt(ptp)_2$ (469 ± 13 ns) is one possible reason for the k_{TTA} reduction by decreasing the probability of triplet-triplet interactions (discussed in Section 3).[18,19,29]

2.3. Triplet-Polaron Annihilation

TPA is a process by which triplet excitons interact with charged molecules (polarons) to lose energy. This process can be described as $^3M^* + M^- \xrightarrow{K_{TPA}} M^{-,*} + M$, where M^- represents an electron-charged molecule and k_{TPA} is the TPA rate constant. In TAPC/$Pt(ptp)_2$ devices, TPA mainly occurs between the excited $Pt(ptp)_2$ molecules and electron-charged $Pt(ptp)_2$ molecules because the neat $Pt(ptp)_2$ layer functions as both the EML and electron-transporting layer (ETL) (Supporting Information Figure S1). This quenching process in neat $Pt(ptp)_2$ can be observed by examining changes in the steady-state PL intensity and transient decay in a $Pt(ptp)_2$-based electron-only device.

Assuming that the rate of TPA is proportional to the charge-carrier density $[n_c]$, the differential equation follows:

$$\frac{d[^3M^*]}{dt} = -\frac{[^3M^*]}{\tau} - k_{TPA}[^3M^*][n_c] \quad (3)$$

According to the established calculation method,[17] the steady-state condition of Equation (3) can be finally expressed as:

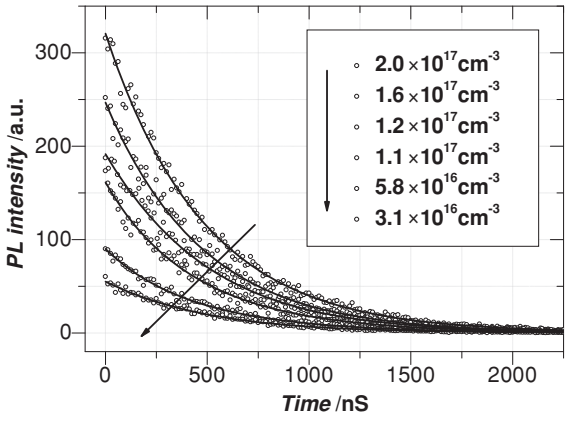

Figure 2. Photoluminescence (PL) time decay of an 100 nm $Pt(ptp)_2$ film (examined at 580 nm) at different excitation intensities indicated by the determined initial exciton density, $[^3M^*(0)]$. The solid lines indicate fitting results using Equation (2). For this measurement, the sample is protected under Ar blanket atmosphere to minimize oxygen quenching during the test. $[^3M^*(0)]$ is determined by the absorption of the film at 337 nm and the laser intensity. It is also assumed that the excitation intensity of the spot is constant in directions normal to the light propagation in the thin film.[17] Furthermore, for this measurement it is assumed an 100% intersystem crossing efficiency for this Pt(II)-based phosphorescent dye,[2,3] which means that only the triplet excitons participate in the emission process.

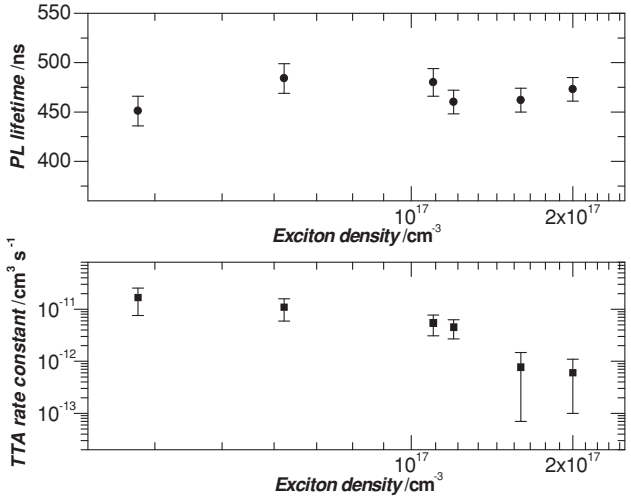

Figure 3. The PL lifetime and triplet-triplet annihilation (TTA) rate constant as a function of initial exciton density [$^3M^*(0)$] in an 100 nm neat $Pt(ptp)_2$ film. Within the experimental error, the calculated lifetime can be recognized as constant in the range of excitation intensity applied to the thin film. The large error of the TTA rate constant partly arises from the determination of $^3M^*(0)$ which is influenced by several sources of error, e.g., the determination of the film thickness, intensity and spot size of the laser beam.

$$\frac{L_{\mathrm{TPA}}(J)}{L_0} = \frac{1}{\left(1 + k_{\mathrm{TPA}}\tau C J^{1/(m+1)}\right)} \tag{4}$$

Here, L_0 is the luminescence intensity in absence of TPA while J is the current density of the single-carrier device. The constant C describes microscopic properties of the specific system (e.g., dielectric constant and carrier mobility).[17] **Figure 4** shows the relative PL intensity of the unipolar device vs current density. The PL intensity decreases with increasing current density, which is associated with the TPA effect in neat $Pt(ptp)_2$. Equation (4) can be used to fit the data plotted (black line),[16,17] from which the value of $k_{\mathrm{TPA}}\tau C$ can be derived.

To measure the magnitude of k_{TPA}, the transient decay of neat $Pt(ptp)_2$ in this electron-only device with changing current density is investigated. In this decay process, TTA and TPA coexist; therefore, the rate of triplet quenching is determined using:

$$\frac{d\left[^3M^*\right]}{dt} = -\frac{\left[^3M^*\right]}{\tau} - k_{\mathrm{TPA}}\left[n_c\right]\left[^3M^*\right] - \frac{1}{2}k_{\mathrm{TTA}}\left[^3M^*\right]^2 \tag{5}$$

Here, the transient decay has linear components and a quadratic component due to bimolecular TTA. k_{TPA} can be obtained by measuring changes in the linear decay rate as a function of current density.[30] **Figure 5**a shows the phosphorescent decay of $Pt(ptp)_2$ in this unipolar device at different electron-current densities; the current density-electric field characteristics of

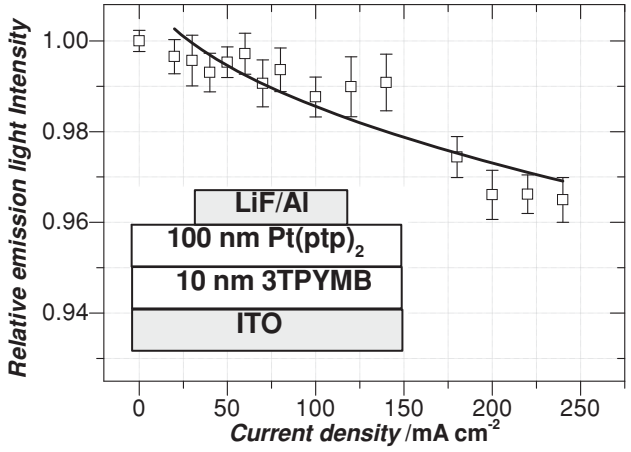

Figure 4. The relative PL intensity of the electron unipolar device (see inset for device structure) under a excitation wavelength of 300 nm. The excitation light is applied through the transparent ITO substrate. The solid line represents the fitting result using Equation (4); its fitting error R^2 is 0.80617. The 10 nm tris[3-(3-pyridyl)mesityl]borane (3TPYMB) is used to avoid anode quenching for excitons and prevent hole injection from ITO.[26a] Under just bias no electroluminescence from $Pt(ptp)_2$ was observed, confirming unipolar electron transport in the device.

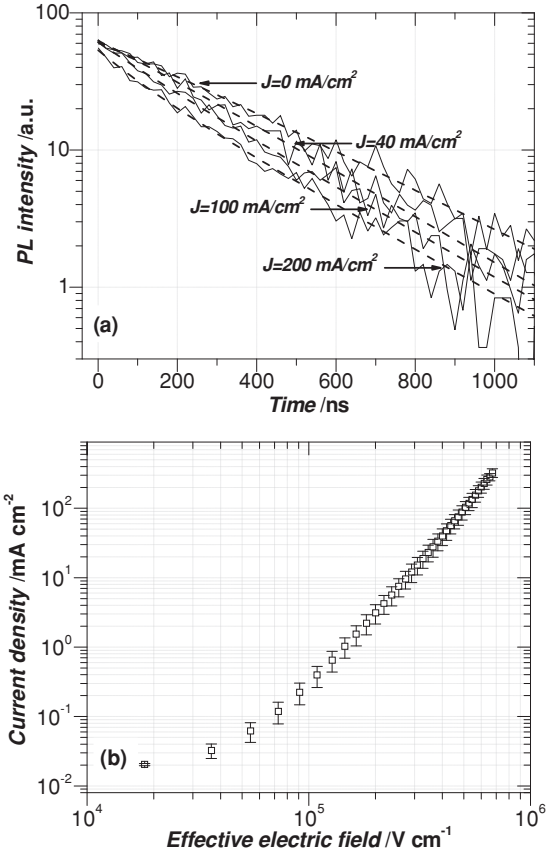

Figure 5. a) The transient PL decay of neat $Pt(ptp)_2$ in response to a pulsed N_2 laser in an electron-only device as a function of electron current density. Device structure is shown in the inset of Figure 4. The laser pulse is applied through the ITO side of the device. b) The current density-electric field characteristics of the electron-only device. In this test, the contribution from 3TPYMB decay can be neglected since the fluorescent lifetime of 3TPYMB is much shorter than the phosphorescent lifetime of $Pt(ptp)_2$.[26a]

this device are shown in Figure 5b. The decreased lifetime with increasing current densities manifests the TPA process. In Equation (5) the value of $k_{TPA}[n_c]$ can be directly obtained by fitting the decay curves in Figure 5a (dashed lines) whereas the electron-carrier density $[n_c]$ can be roughly estimated by fitting Figure 5b data to the equation:[30]

$$J = q\mu_e [n_c] F_{eff} \quad (6)$$

Here, F_{eff} is the effective electric field applied to the neat $Pt(ptp)_2$ layer. **Figure 6** shows the calculated TPA rate $k_{TPA}[n_c]$ and electron-carrier density $[n_c]$ as a function of current density, from which the average value of k_{TPA} of $(1.3 \pm 0.3) \times 10^{-10}$ cm^3 s^{-1} is obtained.[30] Compared to literature values of k_{TPA} ($\approx 10^{-11}$ cm^3 s^{-1}) in doped systems,[15a,17,19,30] the k_{TPA} value in neat $Pt(ptp)_2$ is larger. This is because the neat $Pt(ptp)_2$ film functions as both the EML and ETL here, increasing the likelihood of triplet-polaron interactions in the $Pt(ptp)_2$ layer. Furthermore, we assume that the TPA rate is proportional to the apparent charge-carrier density $[n_c]$. There could be a difference between the calculated vs effective $[n_c]$ in the device that contributes to the TPA process,[17] which could then affect the k_{TPA} value.

2.4. Electric Field-Induced Quenching

Field-induced quenching is a process where electrically-generated excitons, or their precursors prior to exciton formation, are quenched by dissociation into free charges under high electric fields.[20a] To study this quenching process in TAPC/$Pt(ptp)_2$ devices, the effective field F_{eff} applied to the intrinsic $Pt(ptp)_2$ layer needs to be estimated. Because TAPC possesses a high charge (hole) mobility ($\approx 10^{-3}$–10^{-2} cm^2 V^{-1}s^{-1}), in TAPC/$Pt(ptp)_2$ devices the voltagemainly drops across the neat $Pt(ptp)_2$ layer. Therefore, F_{eff} within the device can be defined as follows:[17]

$$F_{eff} = \frac{(U - U_{bi})}{d_{Pt(ptp)_2}} \quad (7)$$

Here, U_{bi} represents the built-in potential and $d_{Pt(ptp)_2}$ the $Pt(ptp)_2$ thickness. U_{bi} can be roughly determined by the difference between the lowest unoccupied molecular orbital (LUMO) level of neat $Pt(ptp)_2$ (or its conduction band edge since its neat films are semiconductors) and highest occupied molecular orbital (HOMO) level of TAPC. In TAPC/$Pt(ptp)_2$ devices, U_{bi} is calculated to be ≈2.1 V (Supporting Information Figure S1) according to equation (7). Accordingly, the upper limit of the device F_{eff} (corresponding to 10^4 cd m^{-2} brightness) is in the 0.40–0.71 MV cm^{-1} range upon variation of the TAPC thickness from 20 to 100 nm. Generally, field-induced quenching is realized in two different manners: amplitude quenching and lifetime quenching.[20a] Both processes can be distinguished by time-resolved measurements. In amplitude quenching, only the precursor to the emissive state is quenched, leading to a decrease of the initial PL amplitude; in lifetime quenching, only the emissive state is quenched, resulting in a shorter lifetime but no reduction of the initial luminescence amplitude.

Time-resolved PL decay measurements were performed to investigate both quenching processes. The device structure employed is ITO/TAPC (50 nm)/$Pt(ptp)_2$ (100 nm)/LiF/Al. A reverse bias is applied to the device to rule out the influence of EL decay since charges cannot be injected into the device. The reverse electric field is increased from zero up to 0.7 MV cm^{-1}, which exceeds the upper limit of device operation conditions (0.3 MV cm^{-1}) by 2×. **Figure 7** shows the PL decays of the device at different F_{eff}. No difference, in either amplitude or lifetime, can be observed up to a field of 0.7 MV cm^{-1}. Therefore, field-induced quenching can be excluded as a cause for the triplet quenching in TAPC/$Pt(ptp)_2$ devices. Similar to our result, field-induced quenching was also found irrelevant to the EQE roll-off as reported by several groups in other OLEDs.[16–18] Although Haneder et al. and Kalinowski et al. both accounted for field-induced quenching process in their devices,[20c,31] it dominated the device EQE roll-off only at very high electric field excitations (>1 MV cm^{-1}). At this point, our experimental results are reasonable since the upper limit of our device operation is below 0.71 MV cm^{-1}.

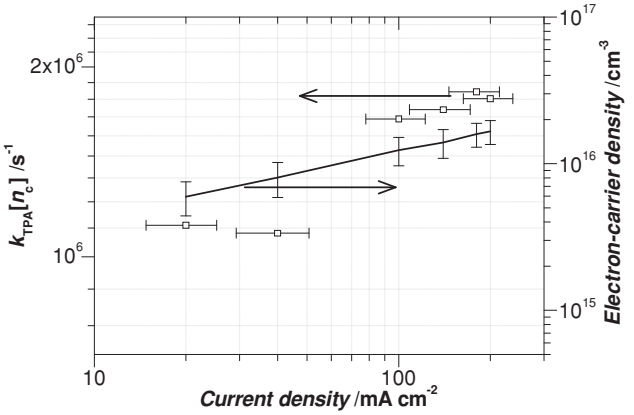

Figure 6. Variation of $k_{TPA}[n_c]$ (k_{TPA}: rate constant of triplet-polaron annihilation) and electron-carrier density $[n_c]$ of the neat $Pt(ptp)_2$-based device (see Figure 4 inset for device structure) with electron current density. $k_{TPA}[n_c]$ is determined from the triplet-polaron quenching data of Figure 5a using Equation (5). $[n_c]$ is calculated from the current density-electric field data of Figure 5b using Equation (6); the electric field-dependent electron mobility of neat $Pt(ptp)_2$ used for the calculation is derived as described in the Supporting Information. The trends of $k_{TPA}[n_c]$ and $[n_c]$ with the current density are very similar to the results by Baldo et al.[30]

3. Discussion

In TAPC/$Pt(ptp)_2$ devices, TAPC can serve as an excellent electron blocker due to its rather high LUMO level (≈2.0 eV). Alternatively, at high electric fields there is a possibility that holes injected from TAPC can traverse the neat $Pt(ptp)_2$ layer to the cathode. Giebink et al. have demonstrated that this current leakage can lead to loss of charge balance and therefore efficiency roll-off.[18,32] To determine whether this process exists in our devices, thanks to a suggestion by an anonymous reviewer, we studied the EL spectra of the device ITO/TAPC (100 nm)/$Pt(ptp)_2$ (80 nm)/tris(8-hydroxy-quinolinato)aluminium (Alq_3) (20 nm)/LiF/Al as a function of electric field. Alq_3 is selected as

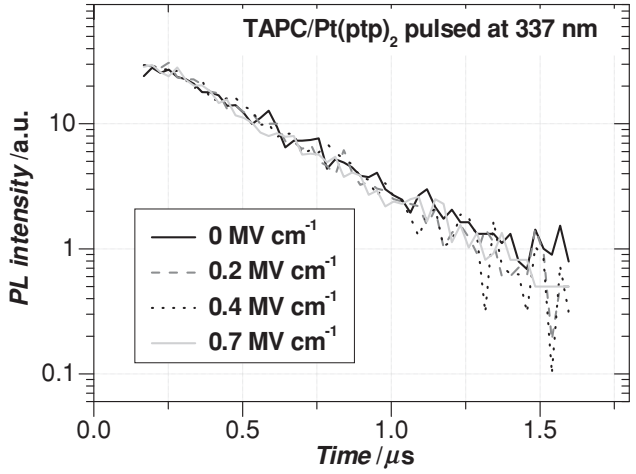

Figure 7. The transient PL decay of a TAPC/$Pt(ptp)_2$ OLED as a function of the effective electric field (F_{eff}) in reverse bias. The device structure is ITO/TAPC (50 nm)/$Pt(ptp)_2$ (100 nm)/LiF/Al. The OLED is excited with a pulsed N_2 laser through the ITO side; and the decay signal is recorded from the peak emission of the device at 580 nm. Here, the decay contribution from TAPC is negligible because TAPC is almost transparent at this excitation wavelength (337 nm).[23]

the sensor layer since it holds a shallow HOMO level of 5.8 eV (see details in Supporting Information Figure S2). If there is significant hole leakage from the neat $Pt(ptp)_2$ layer, the Alq_3 emission will be clearly exhibited in this device. However, no additional emission from Alq_3 is observed during the entire operation (up to 0.9 MV cm^{-1}), as shown in Supporting Information Figure S2, thus excluding the charge leakage process. Therefore, the EQE roll-off of neat $Pt(ptp)_2$ devices is dominated by both the TTA and TPA processes, and contributions from field-induced quenching and charge leakage are ruled out.

Considering both TTA and TPA, the rate equation combining Equations (1) and (3) follows:

$$\frac{d\left[^3M^*\right]}{dt} = -\frac{\left[^3M^*\right]}{\tau} - \frac{1}{2}k_{TTA}\left[^3M^*\right]^2 - k_{TPA}\left[^3M^*\right][n_c] + \frac{J}{qd} \quad (8)$$

Here, d is the thickness of the exciton formation zone (which is kept constant) while q stands for the elementary charge and J/qd describes the exciton generation under EL conditions assuming that triplet generation is proportional to the current density J.[16] The solution to Equation (8) can be represented as:[17]

$$\frac{\eta(J)}{\eta_0} = \frac{qd}{k_{TTA}\tau J}\left[\begin{array}{c}\sqrt{\left(\frac{1}{\tau}+k_{TPA}CJ^{1/(m+1)}\right)^2+\frac{2Jk_{TTA}}{qd}} \\ -\frac{1}{\tau}-k_{TPA}CJ^{1/(m+1)}\end{array}\right] \quad (9)$$

Here, η_0 is the device EQE in absence of TTA and TPA. Equation (9) can be used to model the device EQE as a function of J. Thus, η_0 represents the maximum forward viewing EQE of each device to scale the fitting curves. Furthermore, Equation (9) depends on four parameters that can be used to fit the experimental EQE: k_{TTA}, k_{TPA}, τ and d. The first three parameters, which were quantitatively determined in Section 2, will be implemented into the model calculation, leaving d as the only free parameter. As discussed above, measurement of k_{TTA} was performed at a calculated PL excitation strength $[^3M^*(0)]$ ranging from 10^{16} to 10^{17} cm^{-3}. Here if we assume d is in the range of 1–10 nm for TAPC/$Pt(ptp)_2$ devices, the electric-excited triplet density $[^3M^*(J)]$ is calculated to be 10^{16}–10^{18} cm^{-3}, with J ranging within 0.1–100 mA cm^{-2} (see the Supporting Information for calculation details). This range of exciton density covers the time-resolved PL experiments (10^{16}–10^{17} cm^{-3}) and does not saturate the molecular density (≈10^{21} cm^{-3}) in the neat $Pt(ptp)_2$ film.[6b,16,17,29] Therefore, the mean value of $k_{TTA} = (6.5 \pm 3.2) \times 10^{-12}$ cm^3 s^{-1} is directly used in the model calculation. Furthermore, in TAPC/$Pt(ptp)_2$ devices TPA mainly occurs between the excited and electron-charged $Pt(ptp)_2$ molecules in the neat $Pt(ptp)_2$ layer. Accordingly, the average value of $k_{TPA} = (1.3 \pm 0.3) \times 10^{-10}$ cm^3 s^{-1} is used in Equation (9).

Figure 8 shows the fitting results for EQE of the TAPC/$Pt(ptp)_2$ devices *vs.* TAPC thickness according to Equation (9). One can see that the curves are in good agreement with the experimental data in a wide range of TAPC thicknesses, demonstrating that the combination of both TTA and TPA can fully explain the EQE roll-off behavior of neat TAPC/$Pt(ptp)_2$ devices. Furthermore, from the fitting results we obtained $d \approx 20$ Å for all of these devices. This value is in good agreement with the experimental results reported previously.[6b,33,34] However, Reineke et al. found $d = 100$ Å in an OLED with a doped EML ([Ir(ppy)$_3$]: TCTA = *fac*-tris(2-phenylpyridine)iridium: 4,4′,4″-tris(*N*-carbazolyl)triphenylamine).[17] We interpret this difference as follows: Unlike neat EMLs, the particular dopant in a guest-host EML can significantly influence charge transport and hence the carrier distribution in the recombination zone.[35] It has been shown that TCTA is a hole-transporting material, and that doping TCTA with Ir(ppy)$_3$ increases the electron mobility and decreases the hole mobility by several orders of magnitude.[36] Therefore, the addition of Ir(ppy)$_3$ can extend the exciton recombination zone by enhancing electron transport in the hole-dominated TCTA layer. By contrast, in TAPC/$Pt(ptp)_2$ devices the only mobile carriers in the $Pt(ptp)_2$ layer are electrons[22] and the electron-hole recombination is, consequently, confined within a narrow region near the TAPC/$Pt(ptp)_2$ interface (Supporting Information Figure S1),[33] rendering our calculation result reasonable.

To shed light on future optimization, the influence of the lifetime (τ), quenching rate constants (k_{TTA} and k_{TPA}) and exciton formation zone (d) on device performance is mathematically discussed, assuming that the four parameters are independent of each other.[17] The fitting curve of the TAPC (50 nm)/$Pt(ptp)_2$ (100 nm) device with its corresponding parameters is plotted as the black line in **Figure 9**. Using this data set as the basis, all parameters are varied sequentially in plots Figure 9a–d. One can see that all parameters influence the device efficiency in a certain manner. As expected, a smaller k_{TTA} (Figure 9a) or k_{TPA} (Figure 9b) favors the reduction of efficiency roll-off by decreasing the corresponding triplet-quenching strength. Figure 9c shows that the phosphorescent lifetime τ strongly affects the device efficiency; a shorter lifetime is greatly beneficial to reducing the efficiency roll-off.[37] This is reasonable because the lifetime of triplet participants directly influence TTA and TPA processes; a shorter-lived triplet reduces the chances for encountering with either another triplet or a polaron, thus reducing the probability of the occurrence of TTA and TPA. From a

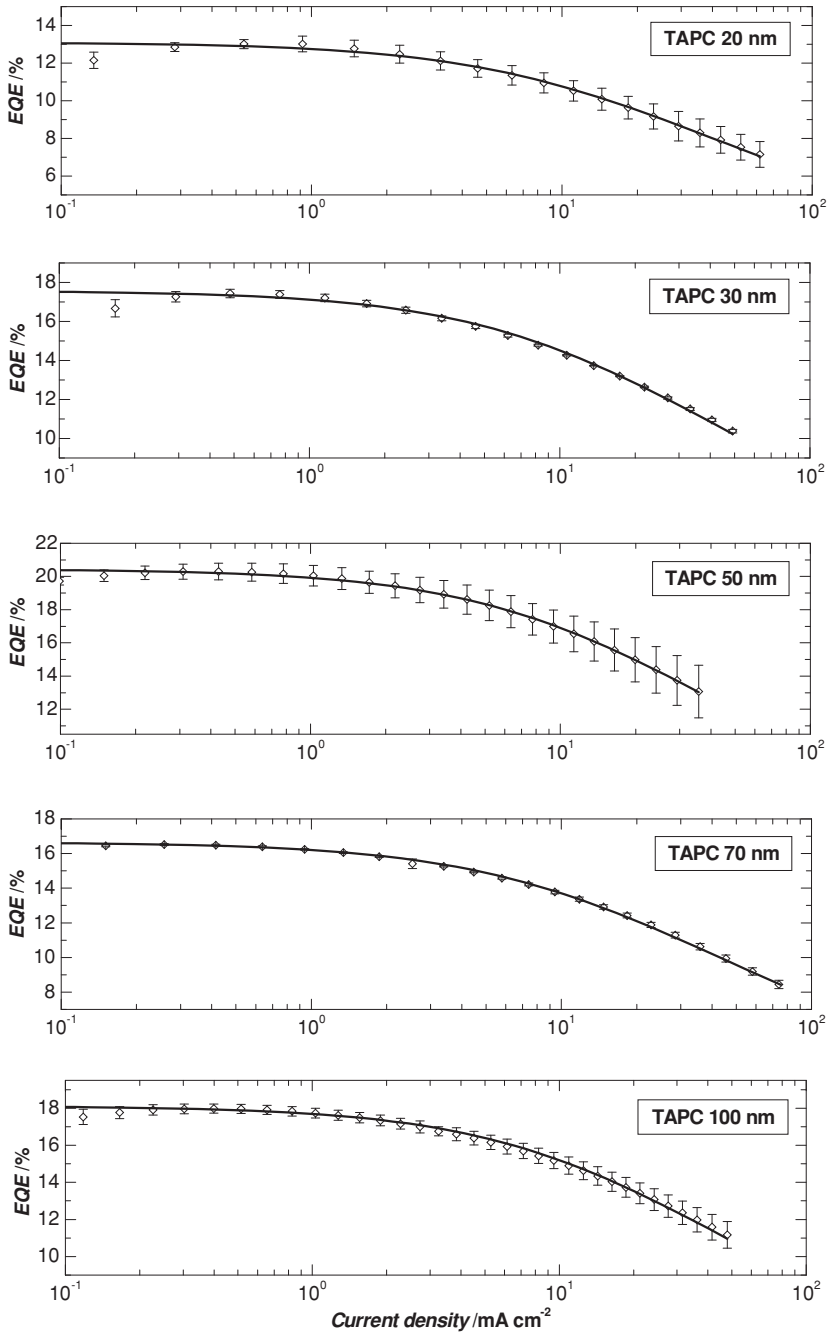

Figure 8. Forward viewing external quantum efficiency (EQE) of ITO/TAPC (≈20–100 nm)/ $Pt(ptp)_2$ (100 nm)/LiF/Al devices with variation of the TAPC thickness. Solid lines represent the fit calculated using Equation (9).

molecular design standpoint, neat $Pt(ptp)_2$ is distinguished vs prototypical 2,3,7,8,12,13,17,18-octaethylporphine platinum (PtOEP), $Ir(ppy)_3$, or tris(1-phenylisoquinoline)iridium [$Ir(piq)_3$] complexes investigated earlier by: (a) there is greater concentration of the heavy metal phosphor in a neat vs doped film; (b) the emission is metal-centered in $Pt(ptp)_2$ neat films[7c] vs ligand-centered in Pt(OEP)[3a] or metal-to-ligand charge transfer in $Ir(ppy)_3$ or $Ir(piq)_3$ doped films;[17,18] and (c) the donor atoms are both nitrogen in the ptp ligand vs the lighter combination of one *N* and one *C* atom in ppy or piq; there are also two other non-donor *N*-heterocyclic atoms in ptp that also contribute to imparting greater heavy atom effect than that in ppy or piq. These factors combine to produce much faster radiative decay in neat $Pt(ptp)_2$ compared to doped films of Pt(OEP), $Ir(ppy)_3$, or $Ir(piq)_3$. Finally, Figure 9d demonstrates that a wider d can reduce efficiency roll-off by decreasing the triplet density, hence triplet-triplet or triplet-polaron interactions, within the exciton formation zone. This is reasonable since the triplet generation density should be the highest therein.

The parameters k_{TTA} and τ are intrinsic properties of neat $Pt(ptp)_2$. Although Zhou et al.[38] have demonstrated that k_{TPA} and d can be optimized by introducing a double-emission layer with different transporting properties, it remains doubtful if both parameters can be tuned in our devices since neat $Pt(ptp)_2$, which serves as both the EML and ETL, is an electron-transporting material. Therefore, further optimization for such DF-PhOLEDs should be focused on exploring phosphors with bipolar transport properties, in addition to shorter phosphorescent lifetimes to further reduce triplet-triplet and triplet-polaron quenching.

4. Conclusions

A non-doped Pt(II)-based PhOLED with a forward viewing EQE of 20.3% and power efficiency of 63.0 lm W^{-1} is demonstrated. The study of triplet quenching processes in the device shows that triplet-triplet and triplet-polaron annihilations (TTA and TPA) account entirely for the efficiency roll-off, and that contributions from charge leakage and field-induced exciton disassociation are insignificant. Both TTA and TPA are studied quantitatively, expressed by the rate constants k_{TTA} and k_{TPA}, respectively. A unified model is introduced to describe the device efficiency roll-off by taking both the TTA and TPA processes into account. According to this model, good agreement with the EQE versus current density characteristics is achieved for a family of $Pt(ptp)_2$ devices. As a next step, the influence of the emitter's lifetime, quenching rate constants and exciton formation zone on the device performance is calculated. The results show that efforts to optimize such non-doped PhOLEDs should concentrate on exploring phosphors with short triplet

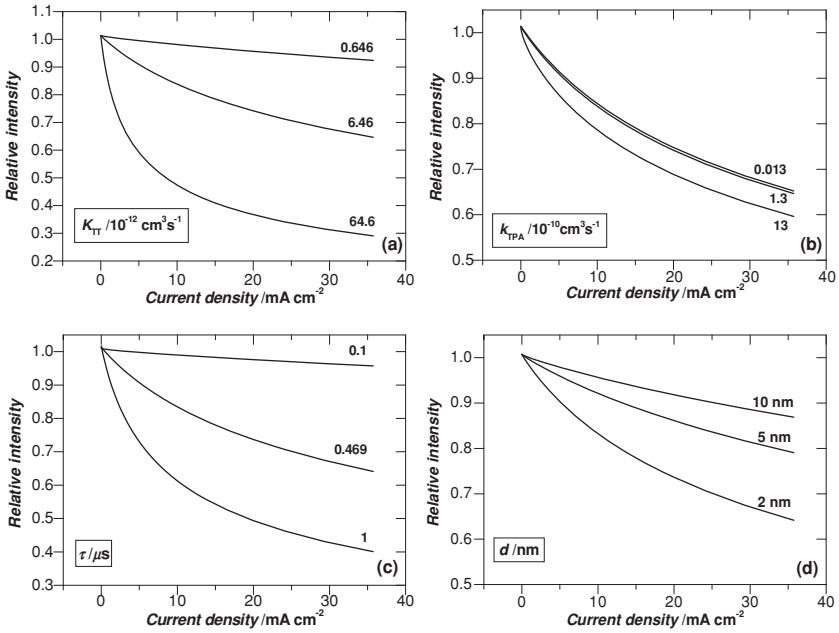

Figure 9. Variation of parameters a) k_{TTA}, b) k_{TPA}, c) τ and d) d using the model calculation. The black line in each plot stands for the fitting curve of the TAPC (50 nm)/$Pt(ptp)_2$ (100 nm) device using Equation (9) (corresponding fitting result is shown in Figure 8). Based on this data, k_{TTA}, k_{TPA}, τ and d are varied consecutively in plots (a–d), respectively. Values used for the four parameters are depicted in each plot.

lifetime and bipolar transport properties, in addition to high quantum yield.

5. Experimental Section

Photoluminescence Characterization: Steady-state photoluminescence spectra were acquired with a PTI Quanta-Master model QM-4 scanning spectrofluorometer. The emission spectra were corrected for the wavelength-dependent xenon lamp intensity and detector response. Time-resolved photoluminescence measurements were acquired using fluorescence subsystem add-ons to the PTI QM-4 instrument. The pulsed excitation source was generated using the 337.1 nm line of the N_2 laser with 1.0 ns pulse width. The output energy density of the N_2 laser is ≈4 μJ cm^{-2}. The absorption spectrum of neat $Pt(ptp)_2$ was obtained using a Perkin Elmer Lambda 900 UV-Vis-NIR system. To avoid contamination by the ambient air and moisture, the samples in time-resolved and steady-state photoluminescence measurements were protected under flowing Ar atmosphere.

Device Fabrication and Characterization: Glass/ITO substrates were cleaned by sonication in a sequential series of solvents, including acetone, 2-propanol and de-ionized water. The substrates were dried with flowing nitrogen after cleaning, and then were treated with oxygen plasma (PLASMALINE 415) for 10 min. The ITO substrate and all organic molecules except $Pt(ptp)_2$ were purchased from Lumtec Ltd., Taiwan. The preparation of $Pt(ptp)_2$ followed procedures previously reported.[7c] The purity of the sample was determined by TGA and elemental analysis. The organic materials were thermally evaporated from Knudsen cells in a high vacuum chamber with a base pressure below 8×10^{-7} Torr (1 Torr = 133.322 Pa). The chamber was vented to load and align the shadow masks for cathode deposition. Quartz crystal oscillators were used to monitor the film thicknesses, which were calibrated ex situ using a profilometer (VEECO DEKTAK VIII). The active area of all devises is 10 mm^2. A calibrated spectrophotometer, PR-650 (PhotoResearch, Inc.), was used to measure the electroluminescence spectrum. A Keithley 2400 source-meter unit linked to a calibrated silicon photodiode, controlled by a LabView interface was used for the measurement of current-voltage-brightness characteristics. All the electroluminescence measurements were carried out in air at room temperature.

Supporting Information

Supporting Information is available from the Wiley Online Library or from the author.

Acknowledgements

This work is supported by the National Science Foundation (CHE-0911690 for electrical characterization and electronic device fabrication aspects; CMMI-0963509 and CHE-0840518 for infrastructure and instrumentation support, respectively) and the Robert A. Welch Foundation (B-1542 for spectroscopy and bonding aspects). We thank an anonymous reviewer for proposing Alq_3 control devices.

Received: February 25, 2013
Revised: April 3, 2013
Published online: May 24, 2013

[1] a) B. W. D'Andrade, R. J. Holmes, S. R. Forrest, *Adv. Mater.* **2004**, *16*, 624; b) G. Schwartz, S. Reineke, T. C. Rosenow, K. Walzer, K. Leo, *Adv. Funct. Mater.* **2009**, *19*, 1319; c) S. Reineke, F. Lindner, G. Schwartz, N. Seidler, K. Walzer, B. Lüssem, K. Leo, *Nature* **2009**, *459*, 234; d) Q. Wang, D. G. Ma, *Chem. Soc. Rev.* **2010**, *39*, 2387; e) M. C. Gather, A. Köhnen, K. Meerholz, *Adv. Mater.* **2011**, *23*, 233; f) M. A. McCarthy, B. Liu, E. P. Donoghue, I. Kravchenko, D. Y. Kim, F. So, A. G. Rinzler, *Science* **2011**, *332*, 570.

[2] C. Adachi, M. A. Baldo, M. E. Thompson, S. R. Forrest, *J. Appl. Phys.* **2001**, *90*, 5048.

[3] a) M. A. Baldo, D. F. O'Brien, Y. You, A. Shoustikov, S. Sibley, M. E. Thompson, S. R. Forrest, *Nature* **1998**, *395*, 151; b) H. Yersin, *Top. Curr. Chem.* **2004**, *241*, 1; c) R. C. Evans, P. Douglas, C. J. Winscom, *Coord. Chem. Rev.* **2006**, *250*, 2093; d) A. Köhler, H. Bässler, *Mater. Sci. Eng., R* **2009**, *66*, 71; e) W.-Y. Wong, C.-L. Ho, *J. Mater. Chem.* **2009**, *19*, 4457.

[4] M. Pfeiffer, S. R. Forrest, K. Leo, M. E. Thompson, *Adv. Mater.* **2002**, *14*, 1633.

[5] a) K. T. Kamtekar, C. Wang, S. Bettington, A. S. Batsanov, I. F. Perepichka, M. R. Bryce, J. H. Ahn, M. Rabinal, M. C. Petty, *J. Mater. Chem.* **2006**, *16*, 3823; b) M.-Y. Lai, C.-H. Chen, W.-S. Huang, J. T. Lin, T.-H. Ke, L.-Y. Chen, M.-H. Tsai, C.-C. Wu, *Angew. Chem. Int. Ed.* **2008**, *47*, 581; c) Z. Ge, T. Hayakawa, S. Ando, M. Ueda, T. Akiike, H. Miyamoto, T. Kajita, M. Kakimoto, *Adv. Funct. Mater.* **2008**, *18*, 584; d) Y. T. Tao, Q. Wang, C. L. Yang, C. Zhong, J. G. Qin, D. G. Ma, *Adv. Funct. Mater.* **2010**, *20*, 2923; e) A. Chaskar, H. F. Chen, K. T. Wong, *Adv. Mater.* **2011**, *23*, 3876; f) Y. H. Zheng, A. S. Batsanov, V. Jankus, F. B. Dias, M. R. Bryce, A. P. Monkman, *J. Org. Chem.* **2011**, *76*, 8300.

[6] a) S. J. Su, E. Gonmori, H. Sasabe, J. Kido, *Adv. Mater.* **2008**, *20*, 4189; b) Q. Wang, J. Q. Ding, D. G. Ma, Y. X. Cheng, L. X. Wang, X. B. Jing, F. S. Wang, *Adv. Funct. Mater.* **2009**, *19*, 84; c) H. Sasabe,

J. Takamatsu, T. Motoyama, S. Watanabe, G. Wagenblast, N. Langer, O. Molt, E. Fuchs, C. Lennartz, J. Kido, *Adv. Mater.* **2010**, *22*, 5003.

[7] a) Y. Kawamura, K. Goushi, J. Brooks, J. J. Brown, H. Sasabe, C. Adachi, *Appl. Phys. Lett.* **2005**, *86*, 071104; b) V. Bulović, R. Deshpande, M. E. Thompson, S. R. Forrest, *Chem. Phys. Lett.* **1999**, *308*, 317; c) M. Li, W.-H. Chen, M.-T. Lin, M. A. Omary, N. D. Shepherd, *Org. Electron.* **2009**, *10*, 863.

[8] a) F.-M. Hsu, C.-H. Chien, C.-F. Shu, C.-H. Lai, C.-C. Hsieh, K.-W. Wang, P.-T. Chou, *Adv. Funct. Mater.* **2009**, *19*, 2834; b) S.-H. Eom, Y. Zheng, E. Wrzesniewski, J. Lee, N. Chopra, F. So, J. G. Xue, *Org. Electron.* **2009**, *10*, 686; c) J.-H. Jou, W.-B. Wang, S.-Z. Chen, J.-J. Shyue, M.-F. Hsu, C.-W. Lin, S.-M. Shen, C.-J. Wang, C.-P. Liu, C.-T. Chen, M.-F. Wu, S.-W. Liu, *J. Mater. Chem.* **2010**, *20*, 8411; d) H.-H. Chou, C.-H. Cheng, *Adv. Mater.* **2010**, *22*, 2468; e) S. O. Jeon, S. E. Jang, H. S. Son, J. Y. Lee, *Adv. Mater.* **2011**, *23*, 1436.

[9] a) M. Ikai, S. Tokito, Y. Sakamoto, T. Suzuki, Y. Taga, *Appl. Phys. Lett.* **2001**, *79*, 156; b) M. Cai, T. Xiao, E. Hellerich, Y. Chen, R. Shinar, J. Shinar, *Adv. Mater.* **2011**, *23*, 3590; c) Z. B. Wang, M. G. Helander, J. Qiu, D. P. Puzzo, M. T. Greiner, Z. W. Liu, Z. H. Lu, *Appl. Phys. Lett.* **2011**, *98*, 073310; d) D. Tanaka, H. Sasabe, Y.-J. Li, S.-J. Su, T. Takeda, J. Kido, *Jpn. J. Appl. Phys.* **2007**, *46*, L10.

[10] a) E. L. Williams, K. Haavisto, J. Li, G. E. Jabbour, *Adv. Mater.* **2007**, *19*, 197; b) Q. Wang, J. Ding, D. Ma, Y. Cheng, L. Wang, F. Wang, *Adv. Mater.* **2009**, *21*, 2397; c) J. H. Seo, S. J. Lee, B. M. Seo, S. J. Moon, K. H. Lee, J. K. Park, S. S. Yoon, Y. K. Kim, *Org. Electron.* **2010**, *11*, 1759; d) J. H. Zou, H. Wu, C.-S. Lam, C. D. Wang, J. Zhu, C. M. Zhong, S. J. Hu, C.-L. Ho, G. J. Zhou, H. B. Wu, W. C. H. Choy, J. B. Peng, Y. Cao, W.-Y. Wong, *Adv. Mater.* **2011**, *23*, 2976; e) B. Zhang, G. Tan, C.-S. Lam, B. Yao, C.-L. Ho, L. Liu, Z. Xie, W.-Y. Wong, J. Ding, L. Wang, *Adv. Mater.* **2012**, *24*, 1873; f) J. Ye, C.-J. Zheng, X.-M. Ou, X.-H. Zhang, M.-K. Fung, C.-S. Lee, *Adv. Mater.* **2012**, *24*, 3410.

[11] a) Y. Sun, N. C. Giebink, H. Kanno, B. Ma, M. E. Thompson, S. R. Forrest, *Nature* **2006**, *440*, 908; b) J. S. Swensen, E. Polikarpov, A. V. Ruden, L. Wang, L. S. Sapochak, A. B. Padmaperuma, *Adv. Funct. Mater.* **2011**, *21*, 3250.

[12] a) S. Tao, Z. Peng, X. Zhang, P. Wang, C.-S. Lee, S.-T. Lee, *Adv. Funct. Mater.* **2005**, *15*, 1716; b) Z. Liu, Z. Bian, L. Ming, F. Ding, H. Shen, D. Nie, C. Huang, *Org. Electron.* **2008**, *9*, 171; c) Q.-X. Tong, S.-L. Lai, M.-Y. Chan, K.-H. Lai, J.-X. Tang, H.-L. Kwong, C.-S. Lee, S.-T. Lee, *Appl. Phys. Lett.* **2007**, *91*, 153504; d) S.-Y. Ku, L.-C. Chi, W.-Y. Hung, S.-W. Yang, T.-C. Tsai, K.-T. Wong, Y.-H. Chen, C.-I. Wu, *J. Mater. Chem.* **2009**, *19*, 773; e) S. Chen, Z. Zhao, B. Z. Tang, H. S. Kwok, *J. Phys. D: Appl. Phys.* **2010**, *43*, 095101; f) W. F. Xie, Z. J. Wu, S. Y. Liu, S.-T. Lee, *J. Phys. D: Appl. Phys.* **2003**, *36*, 2331.

[13] a) Y. Wang, N. Herron, V. V. Grushin, D. LeCloux, V. Petrov, *Appl. Phys. Lett.* **2001**, *79*, 449; b) S.-Y. Chang, J. Kavitha, S.-W. Li, C.-S. Hsu, Y. Chi, Y.-S. Yeh, P.-T. Chou, G.-H. Lee, A. J. Carty, Y.-T. Tao, C.-H. Chien, *Inorg. Chem.* **2006**, *45*, 137; c) Y.-H. Song, S.-J. Yeh, C.-T. Chen, Y. Chi, C.-S. Liu, J.-K. Yu, Y.-H. Hu, P-T. Chou, S.-M. Peng, G.-H. Lee, *Adv. Funct. Mater.* **2004**, *14*, 1221; d) M. Cocchi, J. Kalinowski, L. Murphy, J. A. G. Williams, V. Fattori, *Org. Electron.* **2010**, *11*, 388; e) Z. W. Liu, M. Guan, Z. Q. Bian, D. B. Nie, Z. L. Gong, Z. B. Li, C. H. Huang, *Adv. Funct. Mater.* **2006**, *16*, 1441.

[14] a) X. H. Yang, F.-L. Wu, H. Haveriene, J. Li, C.-H. Cheng, G. E. Jabbour, *Appl. Phys. Lett.* **2011**, *98*, 033302; b) S. Liu, B. Li, L. Zhang, S. Yue, *Appl. Phys. Lett.* **2011**, *98*, 163301.

[15] a) J. Kalinowski, W. Stampor, J. Mężyk, M. Cocchi, D. Virgili, V. Fattori, P. Di Marco, *Phys. Rev. B* **2002**, *66*, 235321; b) I. Tanaka, S. Tokito, *J. Appl. Phys.* **2005**, *97*, 113532; c) W. Staroske, M. Pfeiffer, K. Leo, M. Hoffmann, *Phys. Rev. Lett.* **2007**, *98*, 197402; d) Y. Divayana, X.W. Sun, *Phys. Rev. Lett.* **2007**, *99*, 143003; e) Y. Q. Zhang, G. Y. Zhong, X. A. Cao, *J. Appl. Phys.* **2010**, *108*, 083107; f) D. Song, S. Zhao, H. Aziz, *Adv. Funct. Mater.* **2011**, *21*, 2311.

[16] M. A. Baldo, C. Adachi, S. R. Forrest, *Phys. Rev. B* **2000**, *62*, 10967.

[17] S. Reineke, K. Walzer, K. Leo, *Phys. Rev. B* **2007**, *75*, 125328.

[18] N. C. Giebink, S. R. Forrest, *Phys. Rev. B* **2008**, *77*, 235215.

[19] D. Song, S. Zhao, Y. Luo, H. Aziz, *Appl. Phys. Lett.* **2010**, *97*, 243304.

[20] a) J. Kalinowski, M. Cocchi, D. Virgili, V. Fattori, J. A. G. Williams, *Chem. Phys. Lett.* **2006**, *432*, 110; b) R. J. Holmes, S. R. Forrest, T. Sajoto, A. Tamayo, P. I. Djurovich, M. E. Thompson, *Org. Electron.* **2006**, *7*, 163; c) S. Haneder, E. Da Como, J. Feldmann, M. M. Rothmann, P. Strohriegl, C. Lennartz, O. Molt, I. Munster, C. Schildknecht, G. Wagenblast, *Adv. Funct. Mater.* **2009**, *19*, 2416.

[21] Y. Kawamura, H. Sasabe, C. Adachi, *Jpn. J. Appl. Phys.* **2004**, *43*, 7729.

[22] Q. Wang, I. W. H. Oswald, M. R. Perez, H. P. Jia, B. E. Gnade, M. A. Omary (unpublished).

[23] K. Goushi, R. Kwong, J. J. Brown, H. Sasabe, C. Adachi, *J. Appl. Phys.* **2004**, *95*, 7798.

[24] a) Z. Chen, Q. L. Niu, Y. Zhang, L. Ying, J. B. Peng, Y. Cao, *ACS Appl. Mater. Interfaces* **2009**, *1*, 2785; b) M. G. Helander, Z. B. Wang, J. Qiu, M. T. Greiner, D. P. Puzzo, Z. W. Liu, Z. H. Lu, *Science* **2011**, *332*, 944.

[25] a) M. Li, W.-H. Chen, M.-T. Lin, I. Oswald, M. Omary, N. D. Shepherd, *J. Phys. D: Appl. Phys.* **2011**, *44*, 365103; b) Z. M. Hudson, Z. B. Wang, M. G. Helander, Z. H. Lu, S. N. Wang, *Adv. Mater.* **2012**, *24*, 2922.

[26] a) D. Tanaka, T. Takeda, T. Chiba, S. Watanabe, J. Kido, *Chem. Lett.* **2007**, *36*, 262; b) V. I. Adamovich, S. R. Cordero, P. I. Djurovich, A. Tamayo, M. E. Thompson, B. W. D'Andrade, S. R. Forrest, *Org. Electron.* **2003**, *4*, 77.

[27] R. G. Kepler, J. C. Caris, P. Avakian, E. Abramson, *Phys. Rev. Lett.* **1963**, *10*, 400.

[28] J. Kalinowski, J. Mężyk, F. Meinardi, R. Tubino, M. Cocchi, D. Virgili, *J. Appl. Phys.* **2005**, *98*, 063532.

[29] W. Holzer, A. Penzkofer, T. Tsuboi, *Chem. Phys.* **2005**, *308*, 93.

[30] M. A. Baldo, S. R. Forrest, *Phys. Rev. B* **2001**, *64*, 085201.

[31] J. Kalinowski, W. Stampor, J. Szmytkowski, D. Virgili, M. Cocchi, V. Fattori, C. Sabatini, *Phys. Rev. B* **2006**, *74*, 085316.

[32] B. Ruhstaller, S. A. Carter, S. Barth, H. Riel, W. Reiss, J. C. Scott, *J. Appl. Phys.* **2001**, *89*, 4575.

[33] C. W. Tang, S. A. VanSlyke, C. H. Chen, *J. Appl. Phys.* **1989**, *65*, 3610.

[34] C. Adachi, M. A. Baldo, S. R. Forrest, M. E. Thompson, *Appl. Phys. Lett.* **2000**, *77*, 904.

[35] J. Kalinowski, L. C. Picciolo, H. Murata, Z. H. Kafafi, *J. Appl. Phys.* **2001**, *89*, 1866.

[36] S. Noh, C. K. Suman, Y. Hong, C. Lee, *J. Appl. Phys.* **2009**, *105*, 033709.

[37] T. W. Canzler, J. Kido, *Org. Electron.* **2006**, *7*, 29.

[38] C. X. Zhou, D. S. Qin, M. Pfeiffer, J. Blochwitz-Nimoth, A. Werner, J. Drechsel, B. Maennig, K. Leo, M. Bold, P. Erk, H. Hartmann, *Appl. Phys. Lett.* **2002**, *81*, 4070.